Elastic relaxation behavior, magnetoelastic coupling, and order-disorder processes in multiferroic metal-organic frameworks

R. I. Thomson,[1] P. Jain,[2] A. K. Cheetham,[3] and M. A. Carpenter[1]

[1]*Department of Earth Sciences, University of Cambridge, Downing Street, Cambridge CB2 3EQ, United Kingdom*

[2]*Los Alamos National Laboratory, Los Alamos, New Mexico 87544, USA*

[3]*Department of Materials Science and Metallurgy, University of Cambridge, Pembroke Street, Cambridge CB2 3QZ, United Kingdom*

(Received 3 June 2012; revised manuscript received 3 October 2012; published 21 December 2012)

Resonant ultrasound spectroscopy has been used to analyze magnetic and ferroelectric phase transitions in two multiferroic metal-organic frameworks (MOFs) with perovskite-like structures $[(CH_3)_2NH_2]M(HCOO)_3$ (DMA[M]F, M = Co, Mn). Elastic and anelastic anomalies are evident at both the magnetic ordering temperature and above the higher temperature ferroelectric transition. Broadening of peaks above the ferroelectric transition implies the diminishing presence of a dynamic process and is caused by an ordering of the central DMA ($[(CH_3)_2NH_2]^+$) cation which ultimately causes a change in the hydrogen bond conformation and provides the driving mechanism for ferroelectricity. This is unlike traditional mechanisms for ferroelectricity in perovskites which typically involve ionic displacements. A comparison of these mechanisms is made by drawing on examples from the literature. Small elastic stiffening at low temperatures suggests weak magnetoelastic coupling in these materials. This behavior is consistent with other magnetic systems studied, although there is no change in Q^{-1} associated with magnetic order-disorder, and is the first evidence of magnetoelastic coupling in MOFs. This could help lead to the tailoring of MOFs with a larger coupling leading to magnetoelectric coupling via a common strain mechanism.

DOI: 10.1103/PhysRevB.86.214304 PACS number(s): 75.80.+q, 62.20.D−, 75.85.+t, 77.84.−s

I. INTRODUCTION

Multiferroic materials are of particular current interest due to their potential applications in microwave devices, sensors, transducers, and memory devices.[1–5] The majority of magnetoelectric materials have classically been of the form ABX_3 with the perovskite structure, as in $BiMnO_3$ (Ref. 6) and $BiFeO_3$.[7–10] In these systems the magnetic ordering arises from the unpaired spins of the Mn^{3+} or Fe^{3+} ions, and the ferroelectricity arises due to off center displacements of the lone pair Bi^{3+} ions.[11–13] Ferroelectricity in perovskites classically arises due to displacements of B ions within the BO_6 octahedra leading to a polar distortion as is the case in $BaTiO_3$.[14,15] Alternative mechanisms have been identified in other systems, such as hydrogen bonding order-disorder in lawsonite[16–18] and potassium dihydrogen phosphate.[19]

For the past few years there has been a great deal of attention given to hybrid organic-inorganic porous framework structures, commonly referred to as metal coordination polymers or metal-organic frameworks (MOFs). MOFs have been of interest due to their applications in gas storage/separation and catalysis as well as their photoluminescence and magnetic and electrical properties.[20–28] Interest in ferroelectric and subsequently multiferroic MOFs stems from work by Okada and Sugie[29] who synthesized $Cu(HCOO)_2.4H_2O$ and discovered it to be antiferroelectric, the first instance of such behavior in a MOF. Suzuki and Okada[30] subsequently showed that there may be a temperature range below this transition where the compound becomes ferrielectric. This behavior is accompanied by a transition to a two dimensional antiferromagnet at 17 K (Ref. 31), and therefore this was the first discovery of a multiferroic MOF. Despite this early identification of such phenomena there are only a few reports in the literature of multiferroic MOF materials.[32–34] The ferroelectricity in these MOFs tends to be caused by the ordering of guest/solvent molecules in the pores of the framework.

MOFs based on the formula $[(CH_3)_2NH_2]M(HCOO)_3$ (DMA[M]F with M = Co, Mn, Ni) were originally synthesized by Wang *et al.*[35] who reported space group $R\bar{3}c$ at room temperature, with only very small variations in lattice dimensions between samples. The structure is based on the perovskite architecture with dimethylammonium (DMA) cations placed within the ReO_3 type cavities of the framework forming N-H···O hydrogen bonds to the oxygen atoms of the formate framework. These phases behave as canted antiferromagnets, with ordering temperatures of 8.5, 14.9, and 35.6 K, respectively. DMACoF and DMANiF were also reported to undergo spin reorientation transitions at $T_s = 13.1$ and 14.3 K, respectively. The building block for DMAMnF is shown for reference in Fig. 1.

Jain *et al.*[36] showed that the zinc member of the formate family undergoes a steplike dielectric transition on cooling, with a transition temperature of 160 K. Subsequently, they found that the entire family of compounds displays the same behavior, with transitions in the range 160–185 K.[32,36] The transition is associated with an ordering of the DMA cation in the cavity of the framework from three positions to one, changing the hydrogen bonding motif, as confirmed by vibrational spectroscopy along with a crystallographic study which showed that the low temperature ordered phase belongs to the ferroelectric space group Cc, with associated changes to the framework structure upon ordering.[37] Therefore the transition metal analogs can be considered multiferroic. Above the ferroelectric transition the DMA cations can rotate within the framework, while at lower temperatures, such rotation is frozen, leading to the observed dielectric transition.

Tan *et al.*[38] have shown trends in the mechanical properties of this family of compounds, including an analysis of Young's

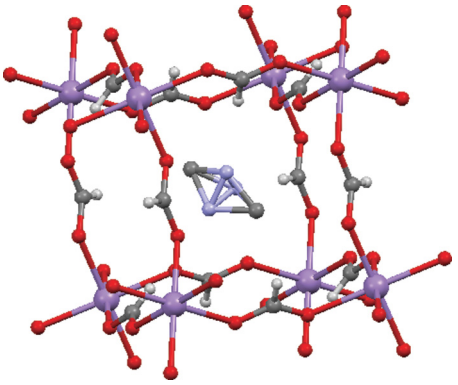

FIG. 1. (Color online) Building block of DMAMnF showing the DMA cation disordered over three positions in the center of the ReO_3 type cavity of the Mn-formate framework. Mn is shown in purple, O in red, C in grey, H in white, and N in blue. Note the disorder of the central nitrogen over three positions. Hydrogens associated with the central cation are omitted for clarity.

modulus, which shows an increase as a function of the crystal field stabilization energy (Ni > Co > Mn = Zn). The focus of this study was the behavior of DMACoF and DMAMnF, which exhibit paraelectric-ferroelectric transition temperatures of 165 and 185 K, respectively.

Magnetoelastic coupling has been identified as a possible mechanism for the magnetoelectric effect,[3] and understanding magnetoelastic coupling in this new family of multiferroics is important with a view to the design of MOFs which might display this desirable property.

II. EXPERIMENTAL METHODS

The experimental resonant ultrasound spectroscopy (RUS) system consists of a single crystal being held lightly between two piezoelectric transducers. The first transducer is driven by a frequency synthesizer at constant amplitude across a range of ultrasonic frequencies (0.1–2 MHz) which in turn causes the sample to resonate at particular frequencies. The second transducer acts as a signal detector which records the response of the sample in terms of its displacement when it is vibrated across the frequency range. Vibrational frequencies detected represent the frequency of normal modes of the sample. The square of a given peak frequency is directly proportional to the elastic constants associated with that normal mode.[39] In the low temperature head the sample is placed lightly across a pair of faces between the two transducers in a mount which is lowered vertically into a helium flow cryostat, as described by McKnight *et al.*[18] Data were collected with the sample chamber filled with a few mbar of helium to allow heat exchange between the sample and the cryostat. Samples of DMACoF and DMAMnF were synthesized according to literature methods.[32]

For DMACoF, RUS experiments were performed on two different crystals. Both were purple and roughly cuboid; the first weighed 4.1 mg and had approximate dimensions $1 \times 1.5 \times 2$ mm, the second weighed 3.5 mg and had dimensions $\sim 1 \times 1 \times 2$ mm. For the first sample the experimental sequence was as follows. The sample was cooled from 290 to 170 K in 30 K steps with a 20 min settle time at each temperature, 170 to 160 K in 1 K steps, 160 to 40 K in 30 K steps, 40 to 20 K in 10 K steps, and 20 to 4 K in 0.5 K steps, and then heated from 4 to 20 K in 0.5 K steps, 20 to 160 K in 5 K steps, 160 to 170 K in 1 K steps, and 170 to 290 K in 5 K steps, all with a 15 min equilibration time at each temperature. 50 000 data points were collected for each spectrum in the frequency range 100–1400 kHz. For the second sample the system was cooled from 290 to 20 K in 30 K steps with a 20 min settle time at each temperature, and 20 to 4 K in 2 K steps. It was then heated from 4 to 20 K in 2 K steps, 20 to 160 K in 5 K steps, 160 to 180 K in 1 K steps, and 180 to 290 K in 5 K steps, all with a 15 min equilibration time at each temperature. Again 50 000 data points were collected for each spectrum in the frequency range 100–1400 kHz.

The sample of DMAMnF used for RUS experiments was white and in the shape of a cube with edge dimensions of $\sim$1 mm and a mass of 2.1 mg. The RUS sequence began with cooling from 290 to 200 K in 30 K steps with a 20 min settle time at each temperature, then from 200 to 175 K in 1 K steps with a 15 min settle time at each temperature, and 175 to 25 K in 30 K steps and 25 to 15 K in 1 K steps, both with a 20 min settle time. The final cooling stage was 15 to 4 K in 1 K steps with a 15 min settle time. The sample was then heated from 4 to 15 K in 1 K steps, 15 to 175 K in 5 K steps, 175 to 200 K in 1 K steps, and 200 to 290 K in 5 K steps, all with a settle time of 15 min at each temperature. For each spectrum the frequency range was 100–1600 kHz and 50 000 data points were collected.

All spectra were transferred to the software package IGOR PRO (WaveMetrics) for analysis. Peak positions and widths at half height were determined for a selection of peaks by fitting with an asymmetric Lorentzian function. The mechanical quality factor Q was calculated using the relationship $Q = f/\Delta f$, where f is the peak frequency and Δf is the width of the peak at half its maximum height. The inverse of the quality factor, Q^{-1}, is a measure of acoustic dissipation (energy loss) in the sample.

III. RESULTS

A. DMACoF

Figure 2 displays a stack of RUS spectra for DMACoF as a function of temperature, with high temperature spectra at the top of the stack and low temperature spectra at the bottom. It is clear that at high temperatures ($>\sim$170 K) there are few broad peaks and at lower temperatures ($<\sim$170 K) many more, sharper peaks are observed. The trend with temperature for the peak at $\sim$400 kHz at 5 K is displayed in Fig. 3, along with marked temperatures for the known phase transitions in this compound. This peak was chosen because it could be followed across the widest temperature range.

It can be seen from Fig. 3 that there are a series of elastic/anelastic anomalies. Above the ferroelectric transition temperature, $\sim$165 K, there is a large increase in the level of dissipation and an associated change in gradient of f^2. This is the characteristic pattern of a Debye relaxation peak for a thermally activated process, for which the temperature dependence of Q^{-1} at a fixed frequency can be described by

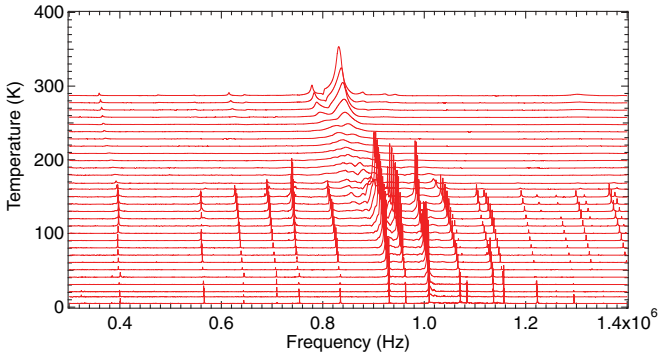

FIG. 2. (Color online) Selected RUS spectra of DMACoF displayed as a stack plot. The y axis should be the amplitude in volts, but the spectra have been offset in proportion to the temperature at which they were collected and the axis is therefore labeled as temperature. Note the disappearance of most peaks above ~170 K.

an expression from Weller *et al.*:[40,41]

$$Q^{-1}(T) = Q_m^{-1}\left\{\cosh\left[\frac{E_a}{Rr_2(\beta)}\left(\frac{1}{T}-\frac{1}{T_m}\right)\right]\right\}^{-1}. \quad (1)$$

Here Q_m^{-1} is the maximum dissipation, T_m is the temperature at the maximum dissipation, R is the gas constant, and $r_2(\beta)$ is the width parameter. The width parameter is a measure of the spread of relaxation times (activation energies) involved in the process, i.e., it indicates whether the Debye-like peak is due to a single relaxation peak or the product of several overlapping peaks indicating multiple relaxations at slightly different frequencies/temperatures. Due to scatter in the Debye-like peak of sample 1, a second RUS run was performed on a different crystal to confirm this behavior and fits to both sets of data are shown in Fig. 3, where a linear baseline was first subtracted from the data to model the general upward trend of Q^{-1}. By fixing $r_2(\beta)$ to be 1, implying a unique relaxation process, the activation energy for the thermally activated process was estimated to be 20 kJ/mol for the first sample and 25 kJ/mol for the second. These values are consistent with the breaking of several hydrogen bonds required to cause disordering of the DMA cation above the ferroelectric transition temperature, and it may be that a dynamical stress applied above the order-disorder temperature can cause changes in the positions of the protons on the time scale of $\sim 10^{-7}$ sec corresponding to the resonance frequency of ~1000 kHz. By way of contrast, there is no sign in the loss behavior of any dynamic microstructure below the transition point. The RUS experiment is showing the diminishing presence of this disorder mechanism on cooling as the frequency of the proton relaxation passes through the frequency of the applied stress at ~210 K.

There is a small anomaly in f^2 at ~40 K and this seems to appear also as a broad peak in Q^{-1}. There is also a small change in gradient of f^2 and an associated discontinuity in the dissipation at ~100 K. These are likely due to further freezing of the motion of the DMA moiety inside the cavity of the framework on cooling below the ferroelectric ordering temperature as described by Besara *et al.*[42] for DMAZnF.

An enlargement of the low temperature region of the f^2 data is shown in Fig. 4. There appears to be a small stiffening associated with the magnetic ordering transition at ~15 K, or the spin reorientation transition at ~13 K, as indicated by deviations from the extrapolation of a baseline of the form

$$f^2_{\text{baseline}} = a_1 + a_2\theta_s \coth\frac{\theta_s}{T} \quad (2)$$

in Fig. 4. This baseline conveniently accounts for saturation as T approaches 0 K in accordance with the third law of thermodynamics (due to the saturation parameter θ_s) and is usually used in describing spontaneous strains.[43–48] Other

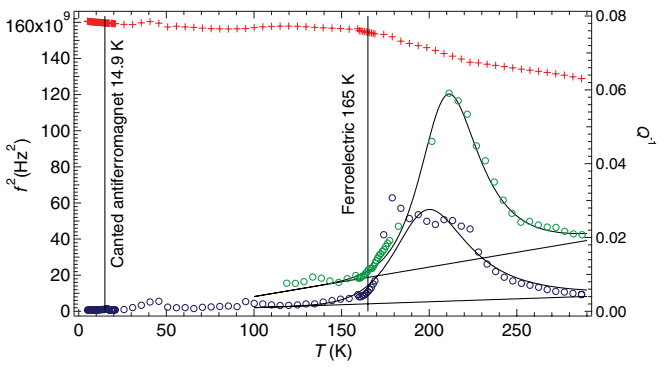

FIG. 3. (Color online) Values of f^2 (red crosses) and Q^{-1} (blue circles) for DMACoF sample 1 and Q^{-1} for sample 2 (green circles). Linear baselines and fits of Eq. (1) to Q^{-1} data shown as solid lines. Fit coefficients for sample 1: $Q_m^{-1} = 0.025$, $T_m = 200$ K, $r_2(\beta) = 1$, and $E_a = 20$ kJ/mol; and for sample 2: $Q_m^{-1} = 0.046$, $T_m = 211$ K, $r_2(\beta) = 1$, and $E_a = 25$ kJ/mol. Temperatures of phase transitions are displayed as vertical black lines.

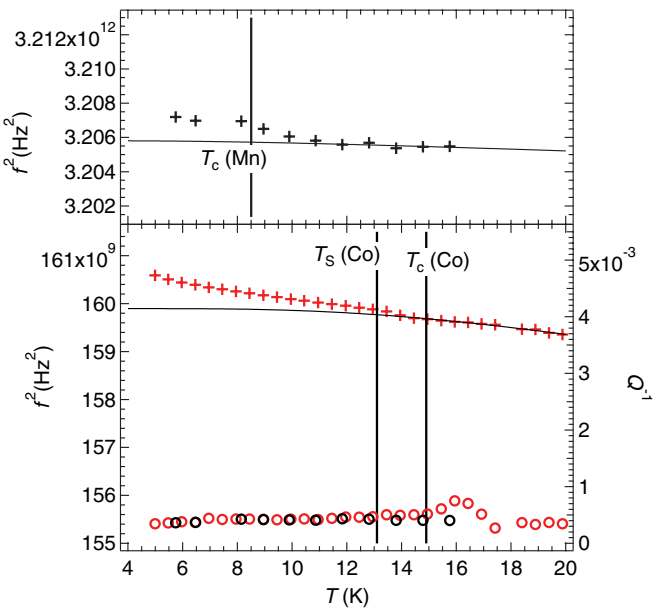

FIG. 4. (Color online) Low temperature values of f^2 (crosses) and Q^{-1} (open circles) for DMACoF (red) and DMAMnF (black) as well of fits of Eq. (2) as solid lines. Fit coefficients for DMACoF are $a_1 = 1.6335 \times 10^{11}$, $a_2 = -1.3136 \times 10^8$, and $\theta_s = 26.244$ K, and for DMAMnF are $a_1 = 3.2065 \times 10^{12}$, $a_2 = -5.8553 \times 10^{17}$, and $\theta_s = 12.462$ K. Transition temperatures are shown as vertical lines. Note the change of scale on the left axis.

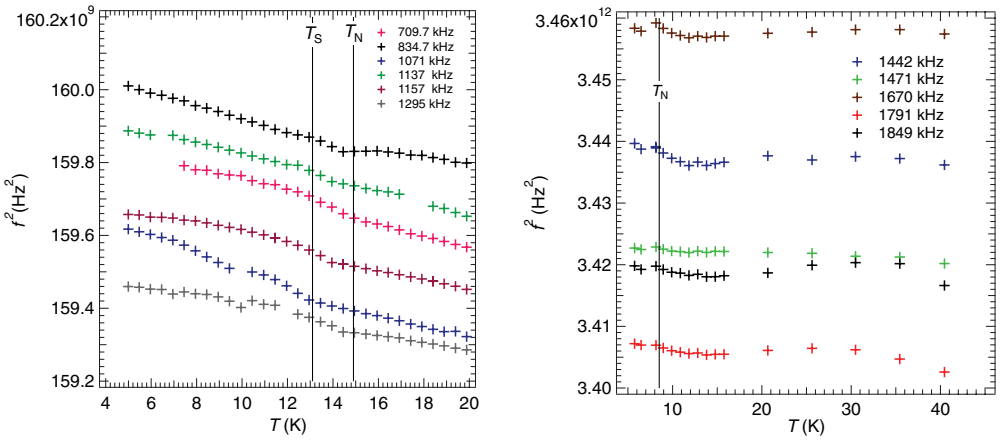

FIG. 5. (Color online) (a) Enlargement of low temperature variations of f^2 for several peaks of DMACoF scaled to appear in the range (159.2–160.2) $\times$ 10^9 Hz^2. (b) Low temperature variation of f^2 for several peaks of DMAMnF scaled to appear in the range (340–346) $\times$ 10^{12} Hz^2. Magnetic transition temperatures are displayed as solid black lines. Peaks are labelled with their frequency values at ~5 K.

peaks analyzed also show this small stiffening [Fig. 5(a)]. There is a small anomaly in the dissipation just above the magnetic ordering temperature for the peak at ~400 kHz but this is at the level of noise. It is not present in other peaks analyzed and therefore probably is not real.

B. DMAMnF

Figure 6 shows the RUS stack for DMAMnF, and Fig. 7 shows the change in the square of the peak frequency and anelastic dissipation for three peaks at 1030 kHz (peak 1), 1641 (peak 2), and 1811 kHz (peak 3) at 5 K as labeled in Fig. 6. From Fig. 6 it is clear that above the ferroelectric transition there are very few broad peaks, but in the low temperature phase many more, sharper peaks are observed. The broadening of peaks in the high temperature phase implies that some change in atomic configurations occurs on the same time scale as the dynamic stress in the RUS experiment. As with DMACoF this is assumed to be related to disorder associated with the hydrogen bonding in the formate framework which facilitates the ferroelectric transition. Movement of the protons under stress is presumably easier in the stability field of the disordered phase than in the stability field of the ordered phase. Figure 7 allows a more exact description of what is happening as temperature is increased.

Peak 1, which could not be followed below ~150 K due to an interaction with another resonance peak, shows stiffening from ~150 K until the ferroelectric transition, at which point there is a discontinuity in f^2 to a lower value. Due to broadening of peaks in the high temperature phase, following peaks through the transition is difficult and this discontinuous behavior is based on the assumption that peak 1 in the high temperature phase matches up with the peak ~1.05 MHz at 5 K in the low temperature phase. This discontinuity in the elastic constants is different from the variation in the Co analog which shows a continuous change through its ferroelectric transition. There is also a discontinuity in the acoustic dissipation of peak 1, with higher losses in the high temperature phase than in the low temperature phase. As with DMACoF this is expected to be related to the dynamics of the DMA cation. Due to the scatter of the data in the temperature interval 200–250 K, an estimate of the activation energy could not be made for this dissipation process, as it was with DMACoF, though it is expected to be

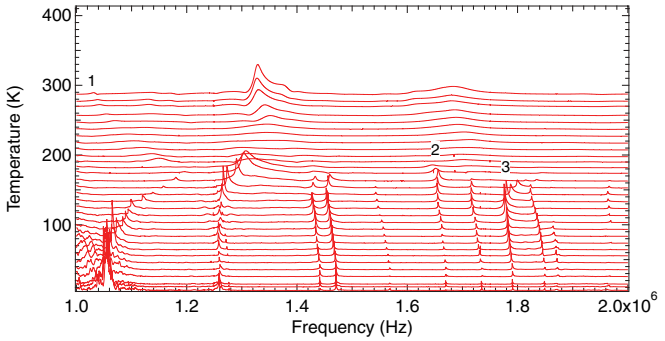

FIG. 6. (Color online) Stack plot of RUS spectra for DMAMnF, with peaks analyzed in Fig. 7 labeled, and spectra offset on the y axis in proportion to the temperature at which they were collected. Some spectra are omitted for clarity.

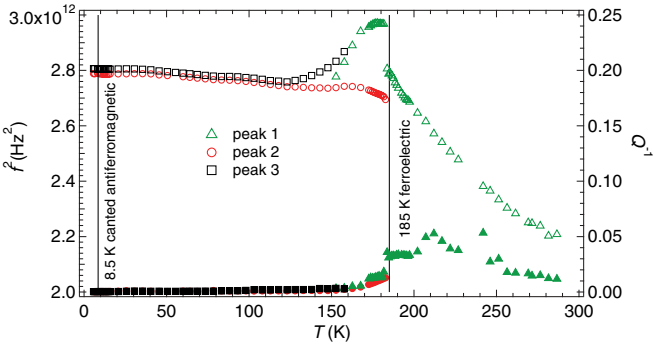

FIG. 7. (Color online) Variation with temperature of f^2 (open symbols) and Q^{-1} (closed symbols) for peaks labeled in Fig. 6. Phase transitions are displayed as black solid lines. Data were scaled so as to overlap at ~10 K.

similar, as the same type of hydrogen bonds need to be broken to allow disorder at high temperatures.

Other peaks could be observed to lower temperatures to analyze behavior associated with magnetic ordering. With increasing temperature from 5 K, peak 3 shows softening to ~120 K at which point stiffening is observed on approaching the ferroelectric transition. Peak 2 shows softening up to ~150 K where there is a small stiffening followed by softening until peaks disappear in the high temperature phase. An enlargement of the low temperature variation of f^2 and Q^{-1} on heating for peak 3 is shown in Fig. 4, and variations of other peaks on heating are displayed in Fig. 5(b). It can be seen that any coupling effect in this compound is much weaker (an order of magnitude) than in DMACoF. A baseline of the form of Eq. (2) was fitted to the data in Fig. 4 to model expected behavior if there were no magnetic ordering. There is then perhaps a slight variation in f^2 at T_c, but this relies heavily on the limited data available below T_c and any anomaly can only be very small. There is no obvious anomaly in the dissipation behavior associated with the magnetic ordering (Fig. 4).

The excess entropy associated with the ferroelectric transition for DMAMnF was reported to be $\Delta S = 0.9$ J/K mol,[32] an order of magnitude less than expected for a complete order-disorder transition. It was therefore suggested that long-range order takes place over a broad temperature range. Heat capacity data from Jain *et al.*[32] for the magnetic ordering in DMAMnF were analyzed to evaluate the excess entropy associated with the magnetic transition at ~8.5 K and are shown in Fig. 8(a). A polynomial baseline

$$C_p = 0.023005T^2 - 0.0002035T^3 \qquad (3)$$

was fit to the heat capacity data (where T is the temperature) and subtracted from C_p to calculate the excess entropy. The total excess entropy [Fig. 8(b)] associated with the magnetic ordering is ~6 J/K mol. This is approximately one-third as much as the expected value for an $S = \frac{5}{2}$ (~15 J/K mol) ordering transition, and there must, therefore, be some further contribution at higher temperature possibly from regions of short-range order, implying that the magnetic transition too occurs over a broad temperature interval.

IV. DISCUSSION

A. Variation in f^2 and Q^{-1}

It is clear from Figs. 4 and 5 that magnetoelastic coupling in these MOFs is weak, with only a very small stiffening associated with decreasing temperature through the magnetic ordering transition in DMACoF and a smaller anomaly in DMAMnF. Although the variation in DMAMnF is not conclusive and, at most, implies a very weak magnetoelastic effect, the variation in DMACoF is more definitive of magnetoelastic coupling. Stiffening behavior correlates with previous studies into magnetoelastic coupling in the frustrated antiferromagnet $YMnO_3$ (Ref. 49) and the canted antiferromagnet β-p-NCC_6F_4CNSSN (Ref. 50) and into proton ordering in the mineral lawsonite.[18] As in β-p-NCC_6F_4CNSSN there is no marked increase or decrease in dissipation associated with the magnetic ordering temperature but, whereas in β-p-NCC_6F_4CNSSN there is an increase in dissipation associated with increasing magnetic disorder, in this case a gentle increase with temperature is observed ~100 K above the transition point associated with the onset of ferroelectricity. It does not appear as though there is any increase in the dissipation in the stability field of the paramagnetic region, as may be expected for an order-disorder process, which may be consistent with regions of short-range order above the transition point consistent with a large contribution to the magnetic entropy above T_c. If there is only very weak spin/lattice coupling, it seems unlikely that there will be much possibility for magnetoelectric coupling, i.e., between the magnetic and ferroelectric order via a common strain mechanism. If stronger magnetoelastic coupling can be achieved, then it follows that coupling between magnetic and electric order parameters could result.

There is a larger increase in Q^{-1} in the paraelectric phase, however, in the form of a Debye-like peak. The scatter in this dissipation peak associated with DMAMnF and the first sample of DMACoF may imply that it could be more accurately

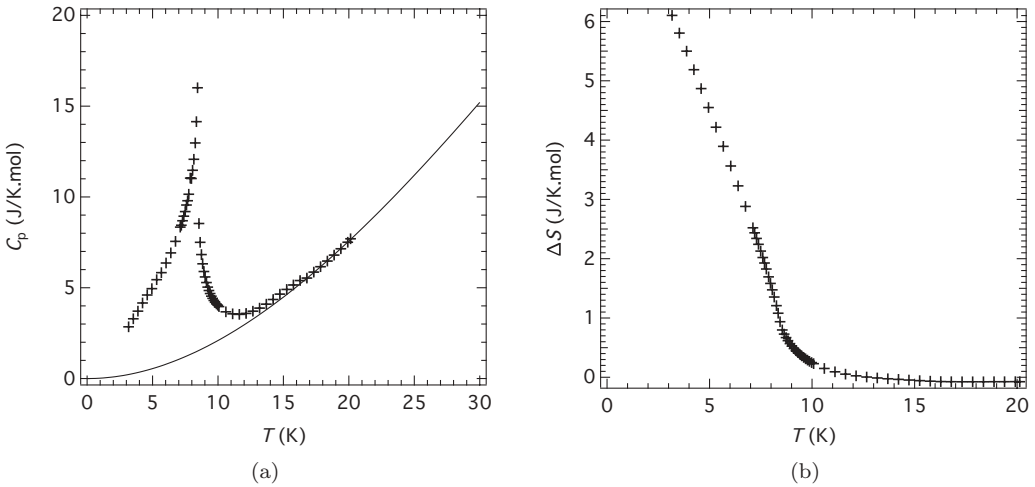

FIG. 8. (a) Fit of Eq. (3) to heat capacity data from Jain *et al.*[32] in the temperature region 0–30 K, and (b) the excess entropy associated with magnetic ordering in DMAMnF.

described by multiple relaxation processes occurring over a temperature range, i.e., that order of the DMA cations does not occur simultaneously at a single temperature but over a broader interval. It was suggested that the ferroelectric transition occurs over a broad temperature range based on the excess entropy[32] and this would be consistent with this view.

B. Origin of ferroelectricity compared with other materials

The ferroelectric behavior due to an order-disorder hydrogen bonding process in both the studied compounds is unlike ferroelectricity in traditional perovskites, where ionic displacement is generally the driving mechanism. Instead it is more reminiscent of the mineral lawsonite $[CaAl_2Si_2O_7(OH)_2{\cdot}H_2O]$ where proton hopping is responsible for ferroelectric ordering.[16–18,51,52] In lawsonite, proton disorder also contributes to a further higher temperature transition and the ordering of different types of protons (hydroxyl and water protons) on different time scales and at different temperatures leads to a wider range of elastic and anelastic anomalies. As in DMAMnF and DMACoF, acoustic dissipation in lawsonite is observed above the proton ordering temperature, and there is no evidence for acoustic losses due to domain walls within the ordered structures. In this study the order-disorder process of the DMA cation hydrogen bonding to the formate framework induces ferroelectric order. Due to the decreased electronegativity of nitrogen compared to oxygen, N-H groups will form weaker hydrogen bonds than O-H groups, and it can be speculated that changing the hydrogen bonding structure within the perovskite cavity to O-H hydrogen bonds, for example, could alter the temperature at which disordering of the cation occurs as a larger activation energy is required to disrupt the O-H hydrogen bonding to the framework and hence affect the ferroelectric transition temperature.

The different origin of ferroelectric ordering between conventional perovskites and MOFs opens up different opportunities for controlling the functionality of the latter. Further ferroelectric and multiferroic materials could be created by changing the organic group within the cavity of the framework.[53] MOFs mimic the perovskite structure but allow for tailored functionality based on the metal ion (for magnetism) and the molecule filling the cavity (for ferroelectricity). However, MOFs tend to have their metal centers further apart than in traditional perovskites, so the magnetic exchange interaction is weak. The introduction of a paramagnetic ion within the cavity may enhance the magnetic communication, while the presence of an organic group to fill the cavity can lead to ferroelectricity. It may be that the introduction of free radicals into the cavity can enhance both magnetic and ferroelectric properties.[33,54] Further investigations into the effect of substituting different groups into the cavity need to be done to analyze the effect on the magnetoelastic coupling with a view to a greater control over functionality of this interesting class of materials.

V. CONCLUSION

RUS has been used to monitor the phase transitions in two DMA[M]F derivatives, M = Co and Mn. Elastic anomalies and an increase in the level of dissipation above the ferroelectric transition are consistent with the view that this is the freezing temperature of a dynamic process associated with the hydrogen bonding conformation between the DMA cation and the formate framework which drives ferroelectric ordering. This mechanism for ferroelectric order differs from the normal displacement of the metal on the B site observed in traditional perovskite materials and means that development of further ferroelectric materials could be made by adjusting the nature of the hydrogen bonding group within the cavity of the framework. A slight elastic anomaly is evident below T_c in DMACoF, in the form of an elastic stiffening, conforming to behavior previously observed in weak ferromagnets and antiferromagnets and observed here in a multiferroic MOF. There appears to be no or very weak magnetoelastic coupling present in DMAMnF. Further tailoring of the functionality of this class of materials leading to stronger strain coupling with magnetic order could result in the much sought after coupling between magnetic and ferroelectric order parameters.

[1] M. Fiebig, J. Phys. D **38**, R123 (2005).
[2] N. A. Spaldin and M. Fiebig, Science **309**, 391 (2005).
[3] W. Eerenstein, N. D. Mathur, and J. F. Scott, Nature (London) **442**, 759 (2006).
[4] J. F. Scott, Nat. Mater. **6**, 256 (2007).
[5] Ce-Wen Nan, M. I. Bichurin, Shuxiang Dong, D. Viehland, and G. Srinivasan, J. Appl. Phys. **103**, 031101 (2008).
[6] A. M. dos Santos, S. Parashar, A. R. Raju, Y. S. Zhao, A. K. Cheetham, and C. N. R. Rao, Solid State Commun. **122**, 49 (2002).
[7] J. R. Teague, R. Gerson, and W. J. James, Solid State Commun. **8**, 1073 (1970).
[8] J. M. Moreau, C. Michel, R. Gerson, and W. J. James, J. Phys. Chem. Solids **32**, 1315 (1971).
[9] D. Lebeugle, D. Colson, A. Forget, M. Viret, P. Bonville, J. F. Marucco, and S. Fusil, Phys. Rev. B **76**, 024116 (2007).
[10] D. Lebeugle, D. Colson, A. Forget, M. Viret, A. M. Bataille, and A. Gukasov, Phys. Rev. Lett. **100**, 227602 (2008).
[11] C. Michel, J.-M. Moreau, G. D. Achenbach, R. Gerson, and W. J. James, Solid State Commun. **7**, 701 (1969).
[12] T. Atou, H. Chiba, K. Ohoyama, Y. Yamaguchi, and Y. Syono, J. Solid State Chem. **145**, 639 (1999).
[13] N. A. Hill, J. Phys. Chem. B **104**, 6694 (2000).
[14] H. D. Megaw, Proc. Phys. Soc. London **58**, 133 (1946).
[15] A. von Hippel, Rev. Mod. Phys. **22**, 221 (1950).
[16] E. Libowitzky and T. Armbruster, Am. Mineral. **80**, 1277 (1995).
[17] E. Libowitzky and G. R. Rossman, Am. Mineral. **81**, 1080 (1996).
[18] R. E. A. McKnight, Michael A. Carpenter, T. W. Darling, A. Buckley, and P. A. Taylor, Am. Mineral. **92**, 1665 (2007).
[19] J. C. Slater, J. Chem. Phys. **9**, 16 (1941).
[20] J. L. C. Rowsell and O. M. Yaghi, Microporous Mesoporous Mater. **73**, 3 (2004).

[21] J. L. C. Rowsell and O. M. Yaghi, Angew. Chem., Int. Ed. **44**, 4670 (2005).
[22] A. K. Cheetham, C. N. R. Rao, and R. K. Feller, Chem. Commun. **2006**, 4780 (2006).
[23] A. K. Cheetham and C. N. R. Rao, Science **318**, 58 (2007).
[24] G. Ferey, Chem. Soc. Rev. **37**, 191 (2008).
[25] T. Yamazaki, Y. Takahashi, and D. Yoshida, J. Colloid Interface Sci. **362**, 463 (2011).
[26] M. Carmen Munoz and J. A. Real, Coord. Chem. Rev. **255**, 2068 (2011).
[27] J. Sculley, D. Yuan, and H. C. Zhou, Energy Environ. Sci. **4**, 2721 (2011).
[28] J. R. Li, Y. Ma, M. C. McCarthy, J. Sculley, J. Yu, H. K. Jeong, P. B. Balbuena, and H. C. Zhou, Coord. Chem. Rev. **255**, 1791 (2011).
[29] K. Okada and H. Sugie, J. Phys. Soc. Jpn. **25**, 1128 (1968).
[30] I. Suzuki and K. Okada, J. Phys. Soc. Jpn. **47**, 1023 (1979).
[31] H. Kobayashi and T. Haseda, J. Phys. Soc. Jpn. **18**, 541 (1963).
[32] P. Jain, V. Ramachandran, R. J. Clark, H. D. Zhou, B. H. Toby, N. S. Dalal, H. W. Kroto, and A. K. Cheetham, J. Am. Chem. Soc. **131**, 13625 (2009).
[33] M. Guo, H. L. Cai, and R. G. Xiong, Inorg. Chem. Commun. **13**, 1590 (2010).
[34] A. Stroppa, P. Jain, P. Barone, M. Marsman, J. Manuel Perez-Mato, A. K. Cheetham, H. W. Kroto, and S. Picozzi, Angew. Chem., Int. Ed. **50**, 5847 (2011).
[35] X. Y. Wang, L. Gan, S. W. Zhang, and S. Gao, Inorg. Chem. **43**, 4615 (2004).
[36] P. Jain, N. S. Dalal, B. H. Toby, H. W. Kroto, and A. K. Cheetham, J. Am. Chem. Soc. **130**, 10450 (2008).
[37] M. Sánchez-Andújar, S. Presedo, S. Yáñez-Vilar, S. Castro-García, J. Shamir, and M. A. Señarís-Rodríguez, Inorg. Chem. **49**, 1510 (2010).
[38] J.-C. Tan, P. Jain, and A. K. Cheetham, Dalton Trans. **41**, 3949 (2012).
[39] A. Migliori and J. L. Sarrao, *Resonant Ultrasound Spectroscopy: Applications to Physics, Material Measurements and Nondestructive Evaluation* (Wiley, New York 1997).
[40] M. Weller, G. Y. Li, J. X. Zhang, T. S. Ke, and J. Diehl, Acta Metall. **29**, 1047 (1981).
[41] R. Schaller, G. Fantozzi, and G. Gremaud, *Mechanical Spectroscopy Q^{-1} with Applications to Materials Science* (Trans Tech, Brandain, Switzerland, 2001).
[42] T. Besara, P. Jain, N. S. Dalal, P. L. Kuhns, A. P. Reyes, H. W. Kroto, and A. K. Cheetham, Proc. Natl. Acad. Sci. USA **108**, 6828 (2011).
[43] H.-W. Meyer, M. A. Carpenter, A. Graeme-Barber, P. Sondergeld, and W. Schranz, Eur. J. Mineral. **12**, 1139 (2000).
[44] P. Sondergeld, W. Schranz, A. V. Kityk, M. A. Carpenter, and E. Libowitzky, Phase Transitions **71**, 189 (2000).
[45] H.-W. Meyer, S. Marion, P. Sondergeld, M. A. Carpenter, K. S. Knight, S. A. T. Redfern, and M. T. Dove, Am. Mineral. **86**, 566 (2001).
[46] M. A. Carpenter, H.-W. Meyer, P. Sondergeld, S. Marion, and K. S. Knight, Am. Mineral. **88**, 534 (2003).
[47] M. A. Carpenter, Am. Mineral. **92**, 309 (2007).
[48] E. K. H. Salje, B. Wruck, and H. Thomas, Z. Phys. B **82**, 399 (1991).
[49] M. Poirier, F. Laliberté, L. Pinsard-Gaudart, and A. Revcolevschi, Phys. Rev. B **76**, 174426 (2007).
[50] R. I. Thomson, E. S. L. Wright, J. M. Rawson, C. J. Howard, and M. A. Carpenter, Phys. Rev. B **84**, 104450 (2011).
[51] E. K. H. Salje, S. Crossley, S. Kar-Narayan, M. A. Carpenter, and N. D. Mathur, J. Phys.: Condens. Matter **23**, 222202 (2011).
[52] E. K. H. Salje and M. A. Carpenter, J. Phys.: Condens. Matter **23**, 112208 (2011).
[53] G.-C. Xu, W. Zhang, X.-M. Ma, Y.-H. Chen, L. Zhang, H.-L. Cai, Z.-M. Wang, R.-G. Xiong, and S. Gao, J. Am. Chem. Soc. **133**, 14948 (2011).
[54] S. V. Potts, L. J. Barbour, D. A. Haynes, J. M. Rawson, and G. O. Lloyd, J. Am. Chem. Soc. **133**, 12948 (2011).